IOP Conf. Series: Journal of Physics: Conf. Series **1249** (2019) 012005 doi:10.1088/1742-6596/1249/1/012005

Wettability analysis of desiccant beads for HVAC systems

Manfredo Guilizzoni, Stefano De Antonellis

Department of Energy, Politecnico di Milano
Via Lambruschini 4, 20156 Milan

manfredo.guilizzoni@polimi.it

Abstract. Vapour adsorption plays a fundamental role in the operation and performance of innovative heat and mass transfer devices for latent heat recovery in HVAC systems. Materials to be used for such devices should present a high affinity with water vapour; at the same time pores should not be flooded in case the surface finds itself in contact with liquid water (e.g., due to moisture formation) and the surface should minimize the wetted parts. From the latter point of view hydrophobic microporous surfaces would be the most suitable; on the contrary, commonly used materials have hydrophilic and/or macroporous surfaces and their behaviour in presence of moisture is still not fully understood. Therefore, this paper is aimed at studying (mostly experimentally, with the support of numerical simulations) wettability and interaction with water, together with adsorption isotherms, of three commercially available desiccant beads (Silica Gel, Silica Gel impregnated with LiCl, Activated Alumina). Results evidence that the behaviour is significantly different between the three materials, even if their static and dynamic wettability is quite similar.

1. Introduction

Innovative devices able to effectively transfer both heat and mass between air streams constitute a fundamental tile for high-performance HVAC applications aiming at energy-saving or nearly-zero-emission buildings. While heat transfer can rely on more consolidated solutions, vapour transfer is still needing active research. Operation and performance of the presently studied heat and mass exchangers for latent heat recovery in HVAC applications heavily depend on vapour adsorption. Materials to be used for such devices should therefore present a high affinity with water vapour, while at the same time the surface pores should not be flooded, and the surface should minimize the wetted parts, in case the surface find itself in contact with liquid water (e.g., due to moisture formation). From the latter point of view, hydrophobic microporous surfaces may be the most suitable; but to promote adsorption, commonly used materials have on the contrary hydrophilic and/or macroporous surfaces. The resulting interactions in presence of moisture are still not fully understood. Therefore, this paper is aimed at studying wettability and dynamic interaction with water, together with adsorption isotherms, of three commercially available desiccant beads for HVAC equipment (Silica Gel, Silica Gel impregnated with LiCl, Activated Alumina). Investigation was experimental, with the support of Computational Fluid Dynamics (CFD) in verifying and tuning the used technique.

2. Investigated materials

Three materials, all of them commercially available and used as obtained by the manufacturer, were selected for the investigation:

- Silica Gel (average pore diameter equal to 20 Å and surface area approximately equal to 800 m^2/g). The material is denoted in this work with SG acronym.
- Silica Gel impregnated with LiCl (Art-Sorb®), denoted as SG-LiCl.
- Activated Alumina (AxSorb®), denoted as AA.

All the materials were used in the form of small beads, having equivalent diameter around 2±0.5 mm. At visual observation (see Fig. 01, pictures taken with a reflex camera with a macro lens) SG beads appear as translucent, in some cases with void inclusions and in others with fusion between two beads; some beads also appear as if they underwent fragile breakage, often evidencing a composite internal structure (a core plus an external shell). They release no powder. SG-LiCL appears similar in shape to SG, but more whitish and not transparent (even if sub-surface scattering seems still present). Finally, AA beads are less uniform in diameter, they seem to be made by pressed powder, white, not transparent and not translucent.

Figure 1. Examples of the investigated beads: SG (left column), SG-LiCl (central column) and AA (right column).

3. Qualitative behaviour in presence of liquid water

Before moving to the quantitative analysis about the wettability of the three surfaces, some results about their qualitative behaviour when placed in contact with liquid water will be summarized. It is first of all confirmed that both SG-LiCl and AA dry beads are covered by a powder layer, which is removed when they enter in contact with liquid water (as it will be shown in figures in the following sections). Such layer and the amount of powder removed are much thicker/larger for AA. On the contrary, SG evidences no such layer. When wet, SG-LiCl beads changes from their original opaque aspect to a much more translucent condition. AA appears significantly more porous of the other materials and when in contact with liquid water it is the only material able to adsorb a large amount (see the image sequence in Fig. 2, first row). On the contrary, after a few seconds (about 10-15 sec) of contact with liquid water, the majority of SG Beads fragment themselves, in most cases with an explosive behaviour (see the image sequence in Fig. 2, second row). This may explain the presence of broken beads cited in the previous section. Further studies are needed to understand the cause of this

phenomenon (e.g., it may be due to residual stresses or to a phase change within the material pores with release of energy).

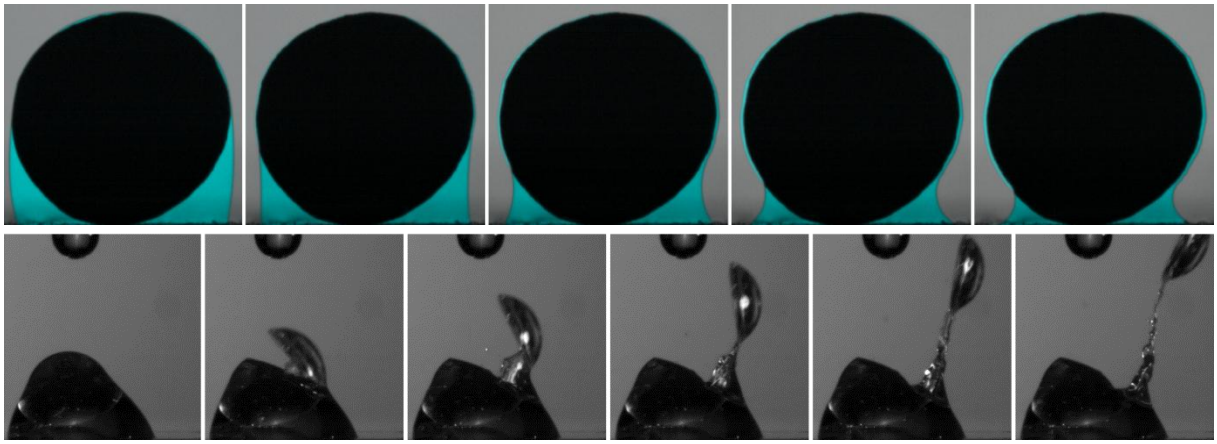

Figure 2. Examples of frames extracted from high-speed videos, showing in the first row AA beads adsorbing liquid water (evidenced in cyan), in the second row SG bead exploding after a few seconds of contact with liquid water.

4. Wettability analysis

4.1. Static contact angle

Wettability of a surface is usually characterized evaluating the contact angle for a sessile (i.e., gently deposed) drop. The contact angle is the angle that the tangent to the drop profile forms with the tangent to the solid surface profile in a plane containing the normal vectors to both the liquid-gas and the solid-gas interfaces. Ideally, for a chemically homogeneous, perfectly flat and smooth surface, in absence of external fields (including gravity) a sessile drop would have a spherical cap shape and the contact angle would be determined only by the three interfacial energies σ_{LV} (between liquid and vapour), σ_{SL} (between solid and liquid), σ_{SV} (between solid and vapour), according to the Young equation [1]:

$$\cos\theta_Y = \frac{\sigma_{SV} - \sigma_{SL}}{\sigma_{LV}} \tag{1}$$

Where θ_Y is the theoretical, thermodynamic equilibrium, contact angle.

In real conditions such angle is both experimentally not accessible and in many cases not reached in itself, e.g., the drop is flattened by gravity and for rough surfaces the Wenzel or Cassie-Baxter wetting states are established [2,3]. In all these cases, conventional measurement techniques return the apparent static contact angle, that summarizes the effects of all the "real world" aspects on the drop shape and contact angle itself. In strict terms, a distribution of values along the contact line (or triple line), i.e., the line along which all the three phases are in contact, should be measured every time that the drop is no longer axisymmetric. Figure 3 panel a) shows an example of a sessile drop on a homogeneous, smooth, flat, horizontal surface with indication of the apparent contact angle.

4.2. Dynamic contact angles

When the drop is not gently deposed on a flat surface, but it impacts onto the surface, or the latter is inclined in presence of gravity, the drop shape and the contact angle change. Focusing on the latter, it becomes larger along the parts of the contact line where the liquid advances or in any cases is in incipient advancement (advancing contact angle θ_{adv}), while it becomes smaller where the liquid is

receding or in incipient recession (receding contact angle θ_{rec}). Again, a distribution of advancing and receding contact angles is observed when the drop is not axisymmetric. The difference between the maximum advancing and minimum receding contact angles is named contact angle hysteresis. Figure 3 panel b) shows an example of a sessile drop on a homogeneous, smooth, flat, vertical surface with indication of the maximum advancing and minimum receding contact angles.

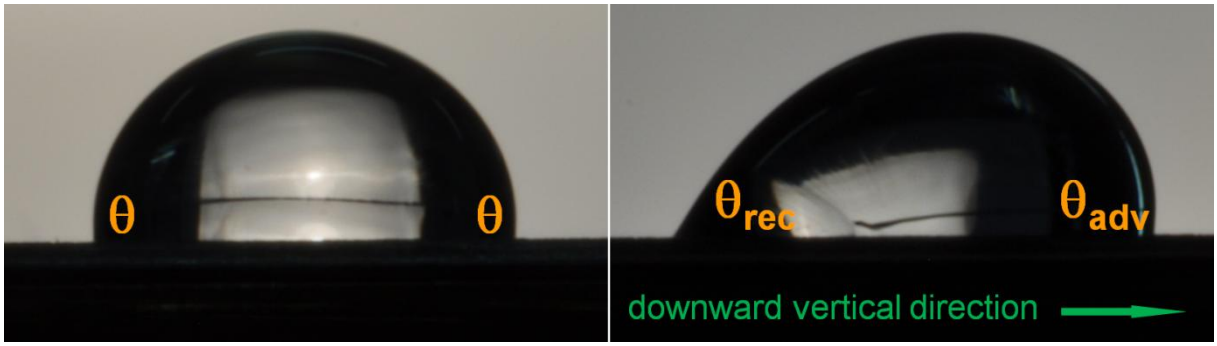

Figure 3. Panel a): sessile drop on a homogeneous, smooth, flat, horizontal surface with indication of the apparent contact angle; panel b) sessile drop on a homogeneous, smooth, flat, vertical surface with indication of the maximum advancing and minimum receding contact angles.

4.3. Wettability analysis performed in this work

Conventional wettability analysis (e.g., Axisymmetric Drop Shape Analysis (ADSA) [4]) is problematic for the surfaces under study, due to such surfaces being hydrophilic, porous and curved. Thus, it is practically impossible to place sessile drops on them. Therefore, water drops were deposed (in fact let fall from a few millimeters, so to have a very low impact velocity) onto the beads, while filming them by means of a high-speed camera (Miro C110 camera equipped with a AF-S Micro NIKKOR 60 mm f/2.8G ED lens) at 1200 fps with exposure time between 38 and 100 μs. Frames from such videos were then processed to evaluate the correlation between the "drop angles" and the "base angles" measured with respect to the horizontal direction in a side view of the drop-surface system:

- The left drop angle is the inclination at the beginning of the drop profile.
- The right drop angle is the inclination at the end of the drop profile.
- The left base angle is the inclination of the base profile at the contact point with the beginning of the drop profile.
- The right base angle is the inclination of the base profile at the contact point with the end of the drop profile.

Frames were extracted using the camera software, then processed using *ad hoc* software to segment the images and to extract the bead, the drop water and their contours. Figure 4 shows an example of a drop-surface system with indication of the cited angles. Figures 5, 6 and 7 show three examples of image sequences from the high speed videos. All the pictures have been processed to increase brightness, sharpness and contrast for better visualization. Figure 5 shows frames from a test with SG with the drop water evidence in light cyan; Fig. 6 shows frames from a test with SG with the contours and contact points superposed to the original images; Fig. 7 shows frames from a test with AA, where it can be seen how the drop removes a powder layer initially present on the bead. Drop and base angles were estimated by linear regression on segments of the drop and base profiles (beginning and end of the drop contour, parts around the contact points for the base contour). For a surface with zero contact angle hysteresis and consequently no dependence of contact angle on the triple line velocity, and, if a perfect measurement with no uncertainty were possible, the drop angle = *f* (base angle) function would be a straight line, with the static contact angle as the intercept, as schematically shown in Fig. 8.

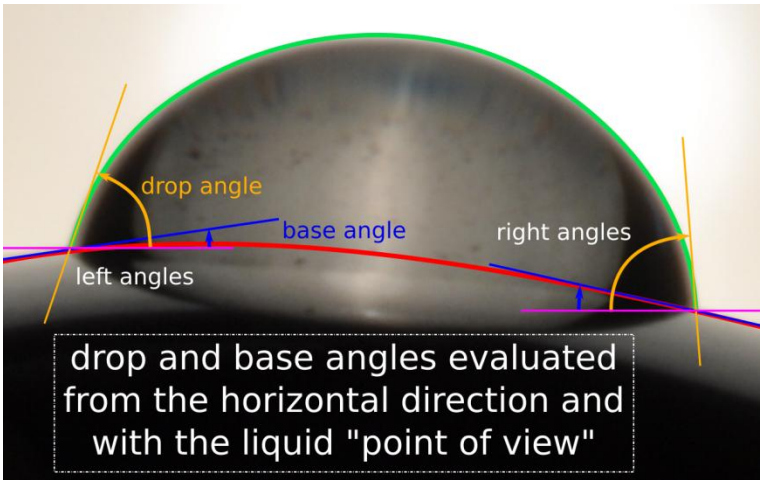

Figure 4. Sketch of a drop-surface system with indication of the drop and base angles.

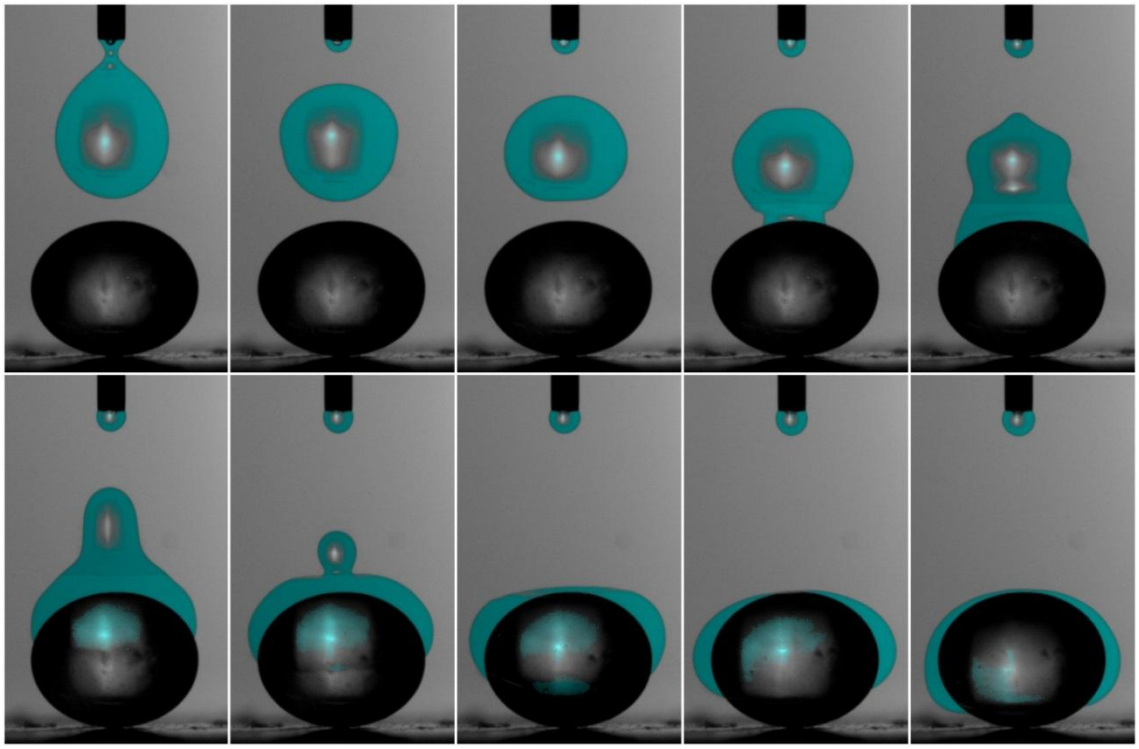

Figure 5. Drop deposition onto a SG bead, with drop water evidenced in cyan. Exposure time 45 μs, time lag between the frames 3.33 ms.

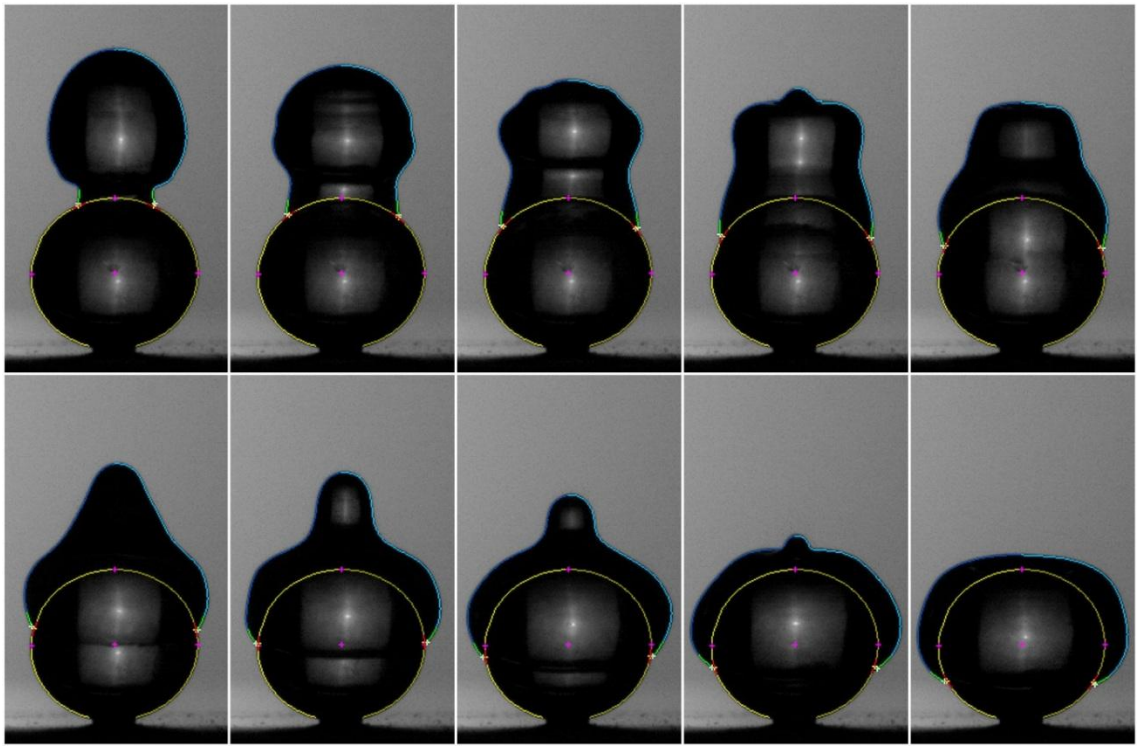

Figure 6. Drop deposition onto a SG bead, with contours, contact points and regression lines evidenced on the picture. Exposure time 43 μs, time lag between the frames 1.67 ms.

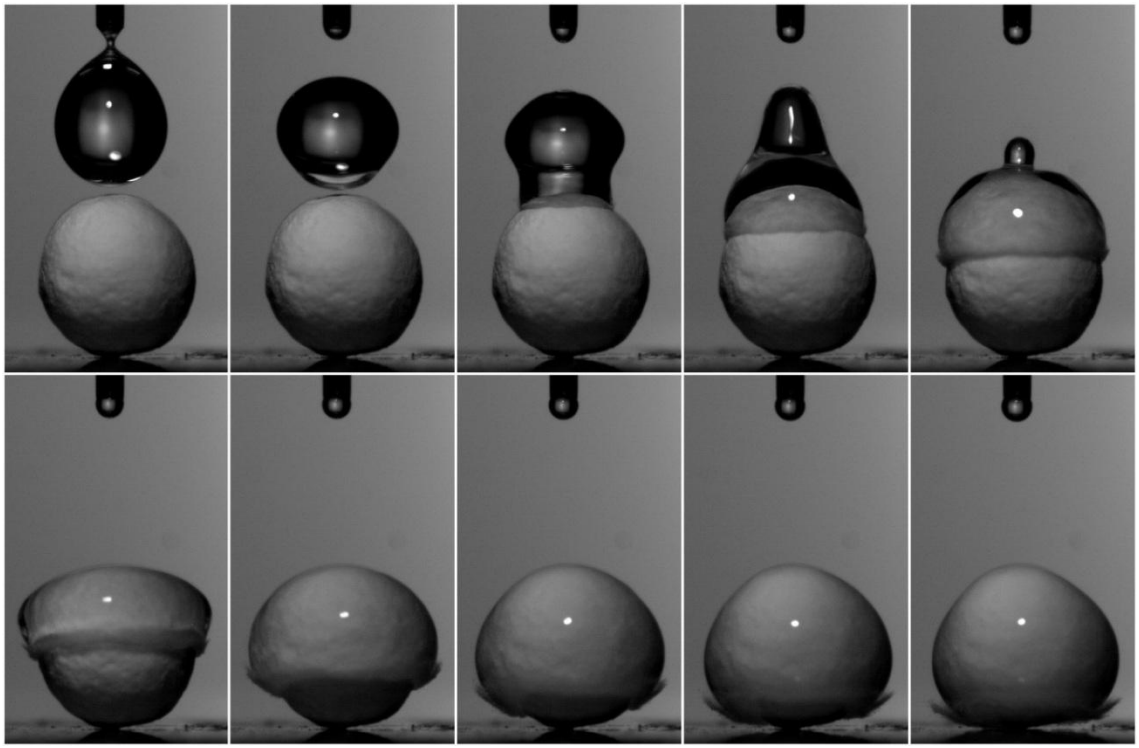

Figure 7. Drop deposition onto an AA bead, evidencing how the drop removes a powder layer from the surface. Exposure time 39 μs, time lag between the frames 4.2 ms.

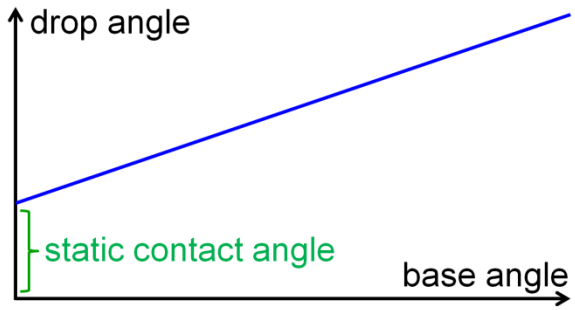

Figure 8. Theoretical drop angle = f (base angle) function for a surface with zero contact angle hysteresis.

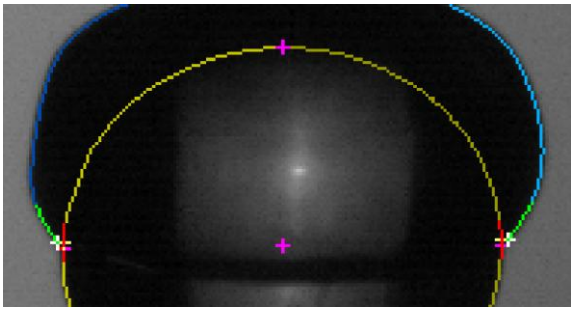

Figure 9. Side view of a drop over a bead, evidencing how the extracted contours are jagged.

In real conditions the situation is more complex due to contact angle hysteresis and to the fact that side view images of the drop-surface system are raster, so both drop and base profiles extracted from such images are jagged (e.g., see Fig. 9). The resulting uncertainty in the measurement of each angle (base and drop) is then much enlarged when calculating the contact angle as their difference, apart from the two peculiar cases in which the base profile is aligned with the horizontal or vertical direction. In the latter cases only the fitting of the drop profile is affected by the jagging and the measurement is more reliable. Due to the experimental procedure, the top and bottom parts of the beads, where their inclination is 0°, are outside of the investigated region. Therefore the contact angle measured (as the difference between the drop angle and the base angle) in correspondence of base angle equal to 90° was selected as the best estimate of the apparent static contact angle. To obtain this, the drop angles in function of the base angles for each experimental set were interpolated using a cubic smoothing spline [5] and the value of the spline for base angle equal to 90° was calculated.

In the proposed technique, many aspects may originate trueness issues:

- Hardware (sensor resolution, lens optical distortions, depth-of-field, light and reflection phenomena, e.g., along the curved drop surface).
- "Software" (bit depth, algorithm and threshold for binarization of the matrix, linear regression to determine the slopes, smoothing spline).

It is practically impossible to place all of them into a mathematical relationship and no reference measurement is available. Therefore a rigorous *a priori* uncertainty analysis could not be performed (this is also why the results will be presented without error bars). Sensitivity analysis about some of the arbitrary parameters in the algorithm was performed using the CFD simulations described in Section 6.

The drop angle = *f* (base angle) and the static contact angle were analyzed for:

- 6 "dry" (in fact in equilibrium with the ambient, not desiccated) SG beads (so 12 sets of points, as left and right evolutions are considered separately).
- 3 “dry” SG-LiCl beads (6 sets).
- 2 "washed-and-dried" (full wetting and free drying in ambient) AA beads (4 sets); washing and drying was needed to remove the powder layer initially covering the AA beads.

5. Adsorption isotherms

Water adsorption isotherms of the desiccant materials were measured by a gravimetric adsorption apparatus (Aquadyne DVS). According to equipment technical specifications, the reference state weight is measured at 80 °C, in nitrogen atmosphere and at ambient total pressure. Water adsorption capacity have been measured at constant temperature and 10% relative humidity step has been adopted (up to 90%).

Adsorption isotherms were evaluated for all the three materials (SG, SG-LiCl and AA). For each material results are the average value obtained by testing three different and randomly selected beads.

6. Validation of the technique for dynamic wettability analysis

A technique to estimate the contact angle on curved surfaces have already been tested for static conditions [6], but validation was needed for its use in dynamic conditions. Given the superposition of dynamic wettability and experimental uncertainty in the available real test cases, the latter are not suited as benchmarks; therefore computational fluid dynamics (CFD) simulations were used. Drop depositions on small spheres with a known constant contact angle boundary condition (namely 15°, 30°, 45°, 60°) were simulated with the Volume of Fluid (VoF) method, using the *interFoam* solver of OpenFOAM [7]. Details about the simulation of drop deposition and impact with *interFoam* can be found in a large number of papers, e.g., see the references in [8]. The settings used for the simulations are the same as those described in [6,8]. A constant contact angle boundary condition was used, which is suitable to model an ideal surface with zero contact angle hysteresis. Two structured axisymmetric meshes were used, with 20250 cells and 81000 cells respectively; the coarser mesh was used for the majority of the simulations, the finer one to assess a very basic mesh independence. A rigorous mesh independence analysis was out of the scopes of the work, as the aim is to obtain images to test the procedure and not fully rigorous results. The base surface and drop external surface were extracted (the latter as the isosurface for volume fraction of water equal to 0.5) and rendered using ParaView [9], thus obtaining images, analogous to the experimental ones, that were processed with the proposed technique. Figure 10 shows an example of frame sequence obtained from CFD results.

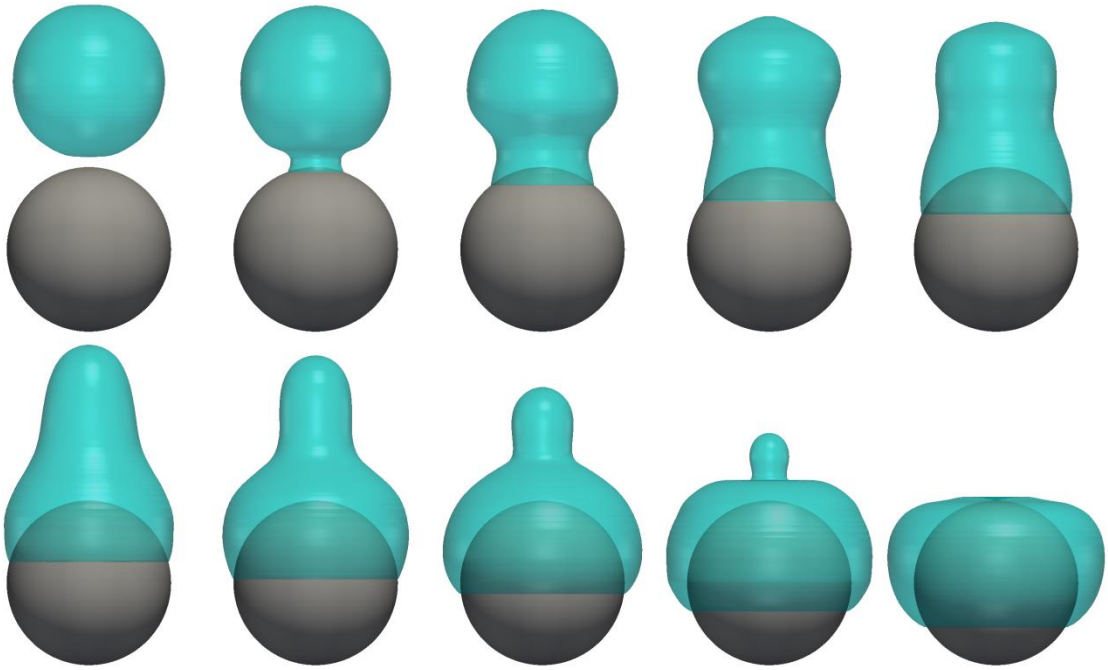

Figure 10. Frame sequence from the CFD simulation of drop deposition onto a sphere having $\theta = 30°$. Time lag between the frames 2 ms.

Figure 11 panel a) shows the drop angle = *f* (base angle) results, including smoothing spline interpolation, for the simulated cases (mesh with 20250 cells). With respect to the ideal straight line, it is evident the different behaviour at the beginning of the drop deposition (low base angles) and near the end of the same (high base angles). It is also evident the data scattering originating from the interface reconstruction and from raster image processing. Despite this dispersion, in all the central part of the deposition transient data from the different simulations are well aligned along separated curves.

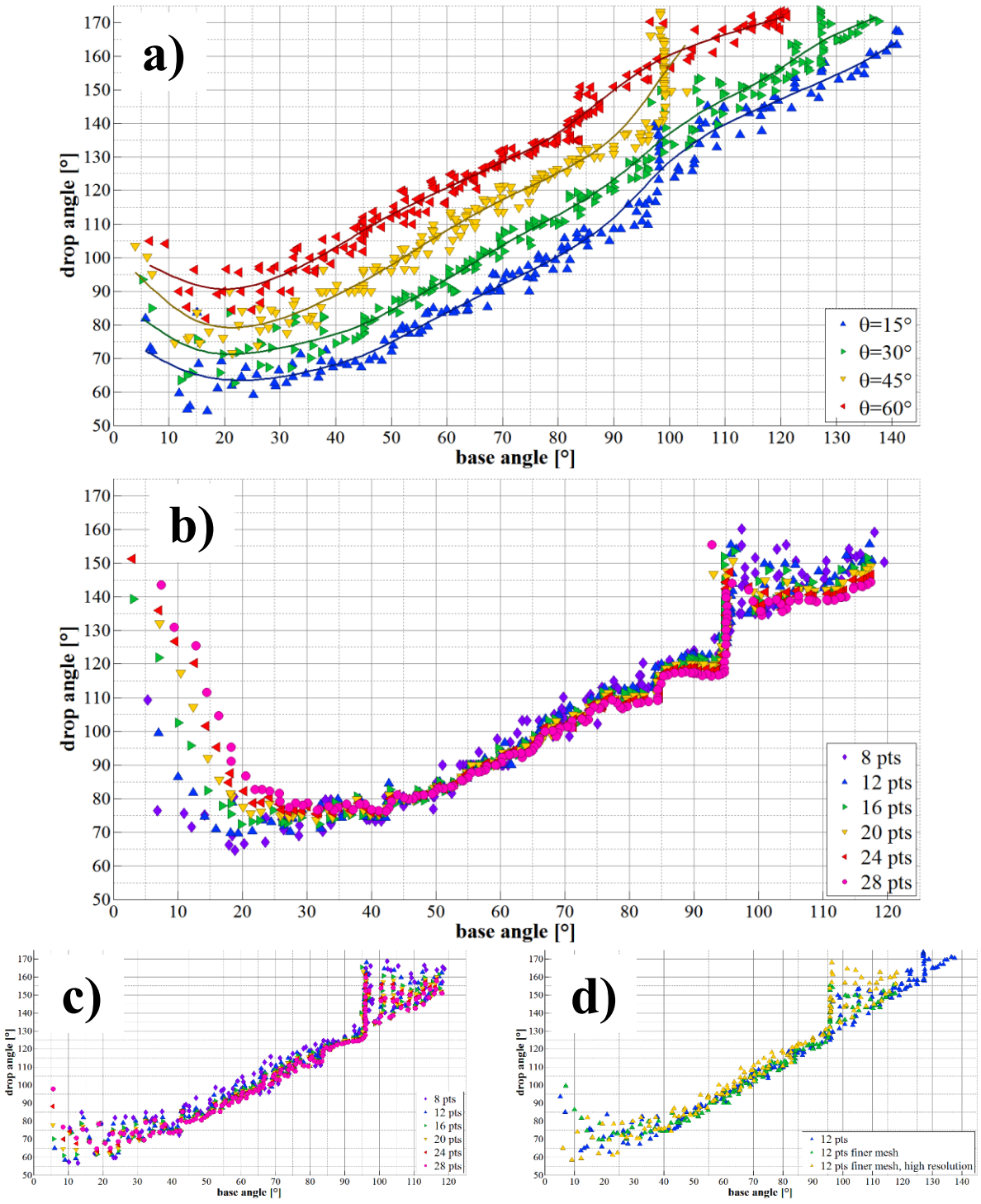

Figure 11. Drop angle = *f* (base angle) function from the results of the CFD simulations. Panel a): results for the investigated contact angles with mesh of 20250 cells, fitting with 12 points and smoothing parameter equal to 10^{-3}; panel b) and c): sensitivity analysis about the influence of the number on points used for the linear fitting evaluated for θ = 30°, mesh with 81000 cells, low-resolution (sphere diameter 275 px) images (panel b) and high-resolution (sphere diameter 975 px) images (panel c); panel d: sensitivity analysis about the influence of the mesh and resolution of the images when using 12 points for the linear fitting.

The overestimation of contact angles in correspondence to base angle 90° is mainly due to the sharp rise the data have during the drop slip along the "positive slope" part of the base surface, that is much larger than in the experimental cases (see the following section), likely due to the zero contact angle hysteresis. CFD analysis also allowed performing a sensitivity analysis on the main "arbitrary" parameter in the procedure, i.e., the image resolution (images with sphere diameter of 275 px and 975 px were evaluated), the number of points used for linear fitting of the selected parts of the drop and surface contours, the value of the smoothing parameter for the cubic smoothing spline. The standard deviation between the estimated contact angle values when changing the latter between 10^{-2} and 10^{-4} is 1.8°. The influence of the other parameters is reported in Fig. 11 panels b), c), d), which evidence how their variation causes a shift of the curves within around 5°. As the resolution in the experimental tests is equal or lower (down to a bead diameter of 150 px) than that of low-resolution CFD images, 12 points and 10^{-4} were the final choices for the number of points for linear fitting of the contours and the value of the smoothing parameter.

7. Experimental results

7.1. Wettability

Figure 12 summarizes all the obtained results, showing the drop angle = *f* (base angle) function for all the investigated beads, together with the CFD results. The behaviour of the three materials appears very similar. More specifically, SG and AA values are practically superposed, while the SG-LiCl data seem slightly higher; in any case, the central part of the experimental trend for all the sets strictly follows the one obtained from numerical simulation with θ = 30°. Concerning the static contact angle, Fig. 13 shows the experimental results with superposed the corresponding three cubic smoothing splines. The contact angle estimated by the latter are 29.8° for SG, 33.8° for SG-LiCl and 26.8° for AA.

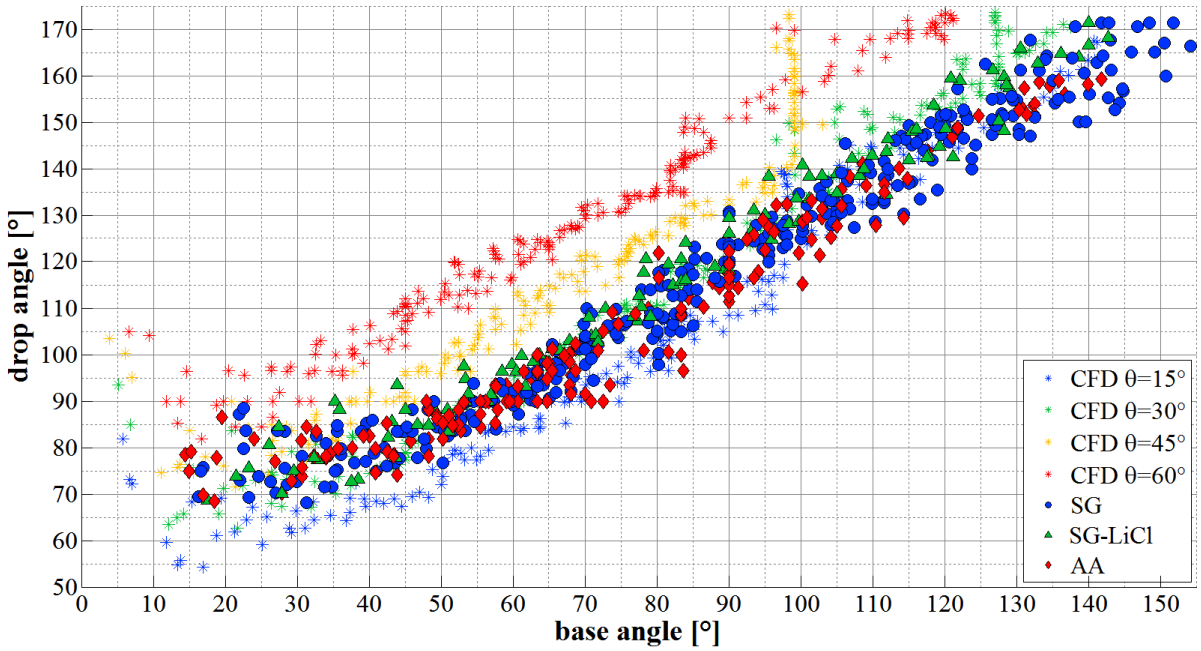

Figure 12. Drop angle = *f* (base angle) function from all the experimental tests, superposed to the CFD results.

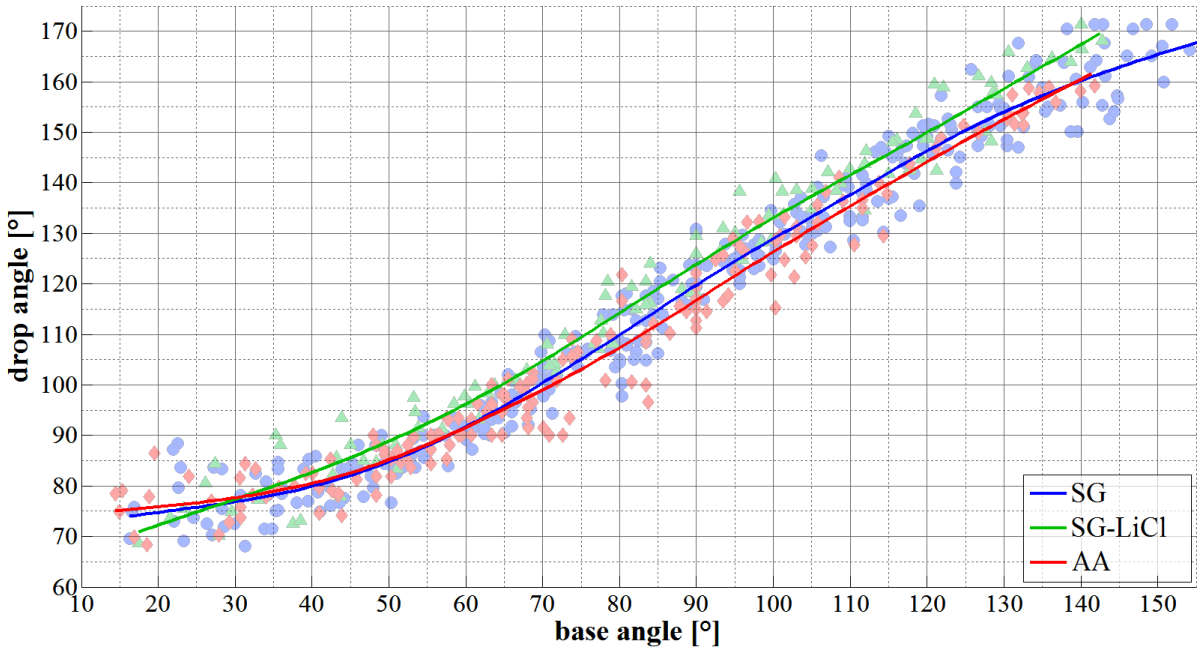

Figure 13. Drop angle = *f* (base angle) function from all the experimental tests, with superposition of the three cubic smoothing splines used to estimate the static contact angle.

7.2. Adsorption isotherms

Figure 14 reports the results in terms of adsorption isotherms, showing the specific adsorbed mass of water as a function of relative humidity at constant temperature for the three investigated materials. The obtained results are in agreement with the literature [10], with a slight underestimation of water uptake, likely due to the procedure used to evaluate reference state: the sample was preliminarily dried at 80 °C in nitrogen atmosphere instead of at 150-200 °C in vacuum condition.

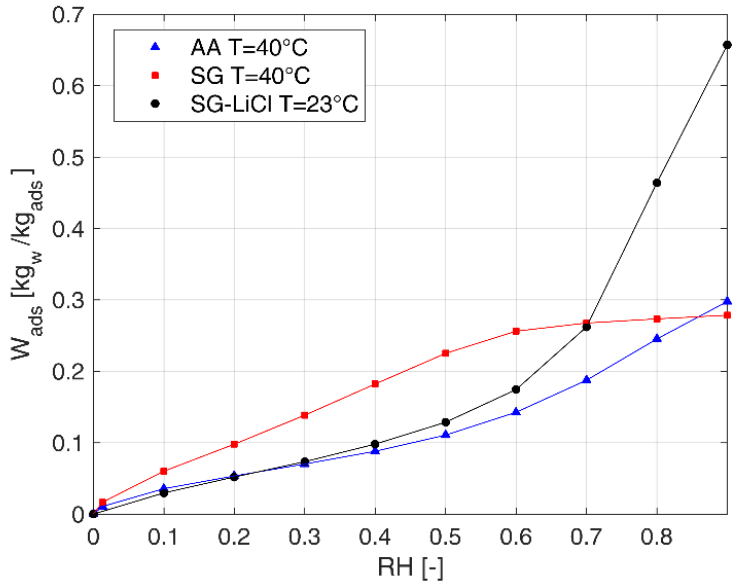

Figure 14. Adsorption isotherms in terms of specific adsorbed mass of water as a function of relative humidity

It can be noticed how the adsorption behaviour is significantly different between the two investigated materials, despite the very similar trends in dynamic wettability and values of the static contact angle.

8. Conclusions

An investigation about the behaviour of three commercially available materials (SG, SG-LiCl and AA) for HVAC in presence of liquid water was carried out. After qualitative observations, drop deposition onto beads was investigated by means of CFD and high speed cinematography to analyse the static and dynamic wettability. The results were compared with adsorption isotherms. The three materials prove to be very similar in terms of wettability (with contact angles in the range 25°-35°), while their adsorption isotherms and qualitative behaviour are very different. SG-LiCl is able to adsorb a large quantity of water compared to SG and AA. In addition, after a few seconds of contact with water the majority of SG beads break in a fragile way or explode. On the other hand, dry AA beads release a large amount of powder.

References

[1] Young T 1805 An essay on the cohesion of fluids *Philos Trans R Soc Lond* **95** 65–87
[2] Wenzel R N 1936 Resistance of solid surfaces to wetting by water *Ind. Eng. Chem.* **28** 988–94
[3] Cassie A B D, Baxter S 1944 Wettability of porous surfaces *Trans. Faraday Soc.* **40** 546–51
[4] del Río O I, Neumann A W 1997 Axisymmetric Drop Shape Analysis: Computational Methods for the Measurement of Interfacial Properties from the Shape and Dimensions of Pendant and Sessile Drops *J. Colloid and Interface Sci* **196(2)** 136–47
[5] de Boor C 1994 A Practical Guide to Splines – Revised Edition Applied Mathematical Sciences Vol. 27 Springer.
[6] Guilizzoni M 2011 Drop shape visualization and contact angle measurement on curved surfaces *J. Colloid Interf. Sci.* **364** 230–6
[7] OpenFOAM <https://www.openfoam.org> (accessed February 2019)
[8] Guilizzoni M, Santini M, Lorenzi M, Knisel V, Fest-Santini S Micro computed tomography and CFD simulation of drop deposition on gas diffusion layers *IOP J. Physics: Conf. Series* **923** (2017) 012013
[9] ParaView <https://www.paraview.org/> (accessed February 2019)
[10] Zheng X, Ge T S, Wang R Z 2014 Recent progress on desiccant materials for solid desiccant cooling systems *Energy* **74** 280–94